

Probing the Type-II Seesaw Mechanism through the Production of Higgs Bosons at a Lepton Collider

Pankaj Agrawal,^{a,b} Manimala Mitra,^{a,b} Saurabh Niyogi,^c Sujay Shil,^{a,b} and Michael Spannowsky^d

^a*Institute of Physics, Sachivalaya Marg, Bhubaneswar, Odisha 751005, India*

^b*Homi Bhabha National Institute, Training School Complex, Anushakti Nagar, Mumbai 400085, India*

^c*Gokhale Memorial Girls' College, Kolkata*

^d*Institute for Particle Physics Phenomenology, Durham University, Durham DH1 3LE, United Kingdom*

E-mail: agrawal@iopb.res.in, manimala@iopb.res.in,
saurabhphys@gmail.com, sujay@iopb.res.in,
michael.spannowsky@durham.ac.uk

ABSTRACT: We investigate the production and decays of doubly-charged Higgs bosons for the Type-II seesaw mechanism at an e^+e^- collider with two center of mass energies, $\sqrt{s} = 380$ GeV and 3 TeV, and analyze the fully hadronic final states in detail. Lower mass ranges can be probed during the 380 GeV run of the collider, while high mass ranges, which are beyond the 13 TeV Large Hadron Collider discovery reach, can be probed with $\sqrt{s} = 3$ TeV. For such a heavy Higgs boson, the final decay products are collimated, resulting in fat-jets. We perform a substructure analysis to reduce the background and find that a doubly-charged Higgs boson in the mass range 800-1120 GeV can be discovered during the 3 TeV run, with integrated luminosity $\mathcal{L} \sim 95 \text{ fb}^{-1}$ of data. For 380 GeV center of mass energy, we find that for the doubly-charged Higgs boson in the range 160-172 GeV, a 5σ significance can be achieved with only integrated luminosity $\mathcal{L} \sim 24 \text{ fb}^{-1}$. Therefore, a light Higgs boson can be discovered immediately during the run of a future e^+e^- collider.

Contents

1	Introduction	1
2	Model Description	3
3	Decay Modes and Experimental Constraints	4
4	Large triplet vev and collider signatures	6
4.1	Low mass $H^{\pm\pm}$ at $\sqrt{s} = 380$ GeV	7
4.2	Boosted Heavy $H^{\pm\pm}$ at $\sqrt{s} = 3$ TeV	10
5	Discussion and Conclusions	15

1 Introduction

With the discovery of the Higgs boson at the Large Hadron Collider (LHC), we start to develop an understanding of how the Standard Model (SM) fermion and gauge boson masses are generated in terms of the Brout-Englert-Higgs (BEH) mechanism. However, one of the main puzzles that still remains unclear is the origin of light neutrino masses and mixings. The same BEH mechanism can, in principle be employed to generate Dirac mass of SM neutrinos by extending the SM to include right-handed neutrinos. However, the required large hierarchy of the Yukawa couplings raises uncomfortable questions. A completely different ansatz is that neutrinos are their own anti-particles and hence, their masses have a different origin than the other SM fermions. A tiny eV Majorana neutrino mass can be generated by the seesaw mechanism, where light neutrinos acquire their masses from a lepton number violating (LNV) $d = 5$ operator $LLHH/\Lambda$ [1, 2]. Such operator is not forbidden as the lepton number is only a classical symmetry of the SM, violated by quantum effects.

There are three proposed categories, commonly known as, Type-I, -II, and -III seesaw mechanisms in which the SM is extended by a $SU(2)_L$ singlet fermion [3–9], $SU(2)_L$ triplet scalar boson [10–13], and $SU(2)_L$ triplet fermion [14], respectively. In particular, the second possibility, i.e., where a triplet scalar field with the hypercharge $Y = +2$ is added to the SM, is the simplest model with an extended Higgs sector. The neutral component of the triplet acquires a vacuum expectation value (vev) v_Δ , and generates neutrino masses through the Yukawa interactions. Perhaps, the most appealing feature of this model is its minimality. The same Yukawa interaction between the lepton doublet and the triplet scalar field generates Majorana masses for the neutrinos, and also dictates the phenomenology of the charged Higgs bosons.

A number of detailed studies have already been performed at the LHC [15–21] to search for the triplet Higgs. One attractive feature of this model is the presence of the

doubly-charged Higgs boson, and its distinguishing decay modes. Depending on the triplet vev, the doubly-charged Higgs boson can decay into same-sign dilepton, same-sign gauge bosons, or even via a cascade decay [15–17]. The details of the Higgs spectrum have been discussed in [22, 23]. For the branching ratios and collider signatures, see [15–19]. The CMS and ATLAS collaborations have searched for the same-sign dilepton final states for all flavors, and constrained the mass of the doubly-charged Higgs as $M_{H^{\pm\pm}} > 820, 870$ GeV at 95% C.L. [24, 25]. However, this is only relevant for a very tiny vev $v_\Delta < 10^{-4}$ GeV, where the doubly-charged Higgs boson decays into the same-sign dilepton with 100% branching ratio. For larger triplet vev such as $v_\Delta \gtrsim 0.01$ GeV, this branching ratio is negligibly small. Therefore, a direct bound on the mass of the $H^{\pm\pm}$ from the same-sign dileptonic final state cannot be obtained. An alternative search where the $H^{\pm\pm}$ is produced in association with two jets (vector boson fusion channel) gives relaxed constraints [26, 27]. For $v_\Delta \geq 10^{-4}$ GeV, the doubly-charged Higgs boson predominantly decays into same-sign diboson. The collider signatures and the discovery prospect of this scenario have been discussed in [28–30], and [31, 32] (see [33] for the discussion on the composite Higgs model and [34] for discussion on flavor violating τ decays). Previous searches for $H^{\pm\pm}$ in the pair-production channel and their subsequent decays into same-sign leptons at LEP-II has put a constraint $M_{H^{\pm\pm}} > 97.3$ GeV at 95% C.L. [35].

While a number of searches at the LHC are ongoing to experimentally verify the presence of the doubly-charged Higgs boson, in this work we perform a detailed collider analysis to explore the discovery prospects at a future lepton collider. For a large mass of the doubly-charged Higgs boson, the pair-production cross-section at the LHC becomes small. Furthermore, the presence of numerous backgrounds weakens its discovery prospects. Therefore, a lepton collider with a much cleaner environment will be more suitable to search the high mass regime of the doubly-charged Higgs boson. In addition, we also exhaust the low mass regime, yet unconstrained by the LHC, and by LEP-II measurements.

We consider the pair-production of the doubly-charged Higgs boson at a lepton collider and its subsequent decays into same-sign gauge bosons. We focus on the hadronic decays of the produced gauge bosons and analyze the multi-jet final states in detail. As a prototype example, we consider the future e^+e^- collider Compact Linear Collider (CLIC) [36–39], that will operate with the center of mass energies $\sqrt{s} = 380$ GeV, 1.4 TeV and 3 TeV. We first analyze the discovery reach of the doubly-charged Higgs boson at 380 GeV center of mass energy. Subsequently, we carry out a detailed simulation for the very heavy doubly-charged Higgs boson with a mass around and beyond one TeV. For such a heavy Higgs, its final decay products are collimated, leading to fat-jets. We perform a jet-substructure analysis and tag the gauge bosons. We find that a heavy Higgs boson with a mass up to 1120 GeV can be most optimally discovered with 5σ significance at the 3 TeV run of CLIC with 95 fb^{-1} of data. For lower masses, the range 160 – 172 GeV can be covered with only $\mathcal{L} \sim 24 \text{ fb}^{-1}$ of luminosity. For the earlier discussions on Higgs triplet model at a linear collider, see [40–43]. For the other SM and BSM searches at CLIC and other linear colliders, see [38, 44–58] for Higgs physics and effective field theory, [59–63] for different BSM scenarios, and [64–70] for seesaw and radiative neutrino mass model searches. For the discussion on probing dark-sector at e^+e^- collider, see [71, 72].

Our paper is organized as follows: we briefly review the basics of the Type-II seesaw model in Sec. 2. In Sec. 3, we discuss existing experimental constraints. In the subsequent subsections, Sec. 4.1 and Sec. 4.2, we analyze in detail the production cross-sections and the discovery potential of the multi-jet final states at the e^+e^- collider. Finally, we present our conclusions in Sec. 5.

2 Model Description

In addition to the SM Higgs field Φ , the Type-II seesaw model [10–13] contains an additional $SU(2)_L$ triplet Higgs field

$$\Delta = \begin{pmatrix} \frac{\Delta^+}{\sqrt{2}} & \Delta^{++} \\ \Delta^0 & -\frac{\Delta^+}{\sqrt{2}} \end{pmatrix} \sim (1, 3, 2). \quad (2.1)$$

We denote the neutral components of the SM doublet and triplet Higgs fields as $\Phi^0 = \frac{1}{\sqrt{2}}(\phi^0 + i\chi^0)$ and $\Delta^0 = \frac{1}{\sqrt{2}}(\delta^0 + i\eta^0)$, respectively. The real scalars ϕ^0 and δ^0 acquire vevs denoted as v_Φ and v_Δ with $v^2 = v_\Phi^2 + v_\Delta^2 = (246 \text{ GeV})^2$. The light neutrino mass is proportional to the triplet vev v_Δ . The new scalar field Δ , being a triplet under $SU(2)$, interacts with the SM gauge bosons. The relevant kinetic term has the form

$$\mathcal{L}_{\text{kin}}(\Delta) = \text{Tr}[(D_\mu \Delta)^\dagger (D^\mu \Delta)], \quad (2.2)$$

with the covariant derivative $D_\mu \Delta = \partial_\mu \Delta + i\frac{g}{2}[\tau^a W_\mu^a, \Delta] + ig' B_\mu \Delta$. The Yukawa interactions of Δ with the lepton fields are

$$\mathcal{L}_Y(\Phi, \Delta) = Y_\Delta \overline{L}_L^c i\tau_2 \Delta L_L + \text{h.c.}. \quad (2.3)$$

In the above, Y_Δ is a 3×3 matrix and c denotes charge conjugation. The triplet field Δ carries lepton number +2 and hence the Yukawa term conserves lepton number. The scalar potential of the Higgs fields Φ and Δ is

$$\begin{aligned} V(\Phi, \Delta) = & m_\Phi^2 \Phi^\dagger \Phi + \tilde{M}_\Delta^2 \text{Tr}(\Delta^\dagger \Delta) + \left(\mu \Phi^T i\tau_2 \Delta^\dagger \Phi + \text{h.c.} \right) + \frac{\lambda}{4} (\Phi^\dagger \Phi)^2 \\ & + \lambda_1 (\Phi^\dagger \Phi) \text{Tr}(\Delta^\dagger \Delta) + \lambda_2 \left[\text{Tr}(\Delta^\dagger \Delta) \right]^2 + \lambda_3 \text{Tr}[(\Delta^\dagger \Delta)^2] + \lambda_4 \Phi^\dagger \Delta \Delta^\dagger \Phi, \end{aligned} \quad (2.4)$$

where m_Φ and \tilde{M}_Δ are real parameters with mass dimension 1, μ is the lepton-number violating parameter with positive mass dimension and λ, λ_{1-4} are dimensionless quartic Higgs couplings.

There are seven physical Higgs states in mass basis, that arise after diagonalization of the scalar mass matrix written in the gauge basis. They are: the charged Higgs bosons $H^{\pm\pm}, H^\pm$, the neutral Higgs bosons h^0, H^0 and A^0 . The two charged scalar fields Φ^\pm of Φ and Δ^\pm of Δ mix to give singly-charged states H^\pm and the charged Goldstone χ^\pm bosons. Similarly, the mixing between the two CP-odd fields (χ^0 and η^0) gives rise to A^0 , and the neutral Goldstone boson ρ^0 . Finally, we obtain the SM Higgs boson (h) and a heavy Higgs boson (H) via the mixing of the two neutral CP-even states Φ^0 and δ^0 .

The physical masses of the doubly and singly charged Higgs bosons $H^{\pm\pm}$ and H^\pm can be written as

$$m_{H^{++}}^2 = M_\Delta^2 - v_\Delta^2 \lambda_3 - \frac{\lambda_4}{2} v_\Phi^2, \quad m_{H^+}^2 = \left(M_\Delta^2 - \frac{\lambda_4}{4} v_\Phi^2 \right) \left(1 + \frac{2v_\Delta^2}{v_\Phi^2} \right). \quad (2.5)$$

The CP-even and CP-odd neutral Higgs bosons h , and H have the physical masses

$$m_h^2 = \mathcal{T}_{11}^2 \cos^2 \alpha + \mathcal{T}_{22}^2 \sin^2 \alpha - \mathcal{T}_{12}^2 \sin 2\alpha, \quad m_H^2 = \mathcal{T}_{11}^2 \sin^2 \alpha + \mathcal{T}_{22}^2 \cos^2 \alpha + \mathcal{T}_{12}^2 \sin 2\alpha. \quad (2.6)$$

In the above \mathcal{T}_{11} , \mathcal{T}_{22} and \mathcal{T}_{12} have the following expressions:

$$\mathcal{T}_{11}^2 = \frac{v_\Phi^2 \lambda}{2}, \quad \mathcal{T}_{22}^2 = M_\Delta^2 + 2v_\Delta^2 (\lambda_2 + \lambda_3), \quad \mathcal{T}_{12}^2 = -\frac{2v_\Delta}{v_\Phi} M_\Delta^2 + v_\Phi v_\Delta (\lambda_1 + \lambda_4). \quad (2.7)$$

The CP-odd Higgs field A^0 has the mass term

$$m_A^2 = M_\Delta^2 \left(1 + \frac{4v_\Delta^2}{v_\Phi^2} \right), \quad \text{with} \quad M_\Delta^2 = \frac{v_\Phi^2 \mu}{\sqrt{2} v_\Delta}. \quad (2.8)$$

The difference between $H^{\pm\pm}$ and H^\pm masses is dictated by the coupling λ_4 of the scalar potential. For a positive λ_4 , the $H^{\pm\pm}$ is lighter than H^\pm . The mass difference ΔM^2 is

$$\Delta M^2 = M_{H^\pm}^2 - M_{H^{\pm\pm}}^2 \sim \frac{\lambda_4}{2} v_\Phi^2 + \mathcal{O}(v_\Delta^2). \quad (2.9)$$

Throughout our analysis, we consider the mass hierarchy $M_{H^{\pm\pm}} < M_{H^\pm}$.

Due to the non-trivial representations of Δ , the Higgs triplet has interactions with a number of SM fermions and gauge bosons. This opens up a number of possible decay modes that can be explored at the LHC, and at future linear colliders. In the next section, we summarize the different direct experimental constraints on the doubly-charged Higgs boson mass and triplet vev.

3 Decay Modes and Experimental Constraints

The most characteristic feature of the Type II seesaw model is the presence of the doubly-charged Higgs boson $H^{\pm\pm}$, that can decay into the leptonic or bosonic states and gives unique signatures at high energy colliders. The different decay modes and the branching ratios of the $H^{\pm\pm}$ depend on the triplet vev v_Δ . For smaller triplet vev, the $H^{\pm\pm}$ predominantly decays into the same-sign leptonic states $H^{\pm\pm} \rightarrow l^\pm l^\pm$, whereas for larger v_Δ , the gauge boson mode $H^{\pm\pm} \rightarrow W^\pm W^\pm$ becomes dominant [15, 16]. The relevant decay widths are calculated to

$$\Gamma(H^{\pm\pm} \rightarrow l_i^\pm l_j^\pm) = \Gamma_{l_i l_j} = \frac{M_H^{\pm\pm}}{(1 + \delta_{ij}) 8\pi} \left| \frac{M_{\nu_{ij}}}{v_\Delta} \right|^2, \quad M_\nu = Y_\Delta v_\Delta, \quad (3.1)$$

$$\Gamma(H^{\pm\pm} \rightarrow W^\pm W^\pm) = \Gamma_{W^\pm W^\pm} = \frac{g^2 v_\Delta^2}{8\pi M_{H^{\pm\pm}}} \sqrt{1 - \frac{4}{r_W^2}} [(2 + (r_W/2 - 1)^2)]. \quad (3.2)$$

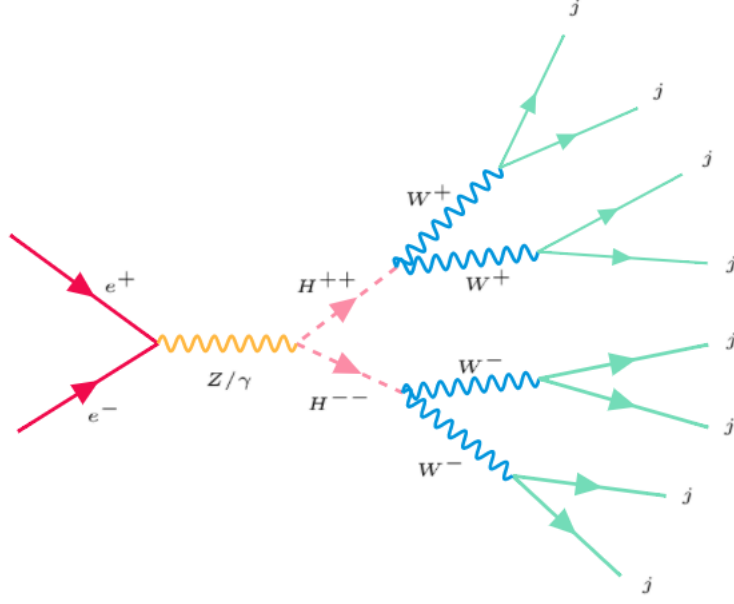


Figure 1. The Feynman diagram for $H^{++}H^{--}$ pair-production and its subsequent decays into gauge bosons.

In the above M_ν denotes the neutrino mass matrix, i, j are the generation indices, $\Gamma_{l_i l_j}$ and $\Gamma_{W^\pm W^\pm}$ are the partial decay widths for the $H^{\pm\pm} \rightarrow l_i^\pm l_j^\pm$, and $H^{\pm\pm} \rightarrow W^\pm W^\pm$ channels, respectively. The parameter r_W denotes the ratio of $H^{\pm\pm}$ and the W gauge boson masses, $r_W = \frac{M_{H^{\pm\pm}}}{M_W}$. The branching fraction of the leptonic and bosonic mode becomes equal around the triplet vev $v_\Delta \sim 10^{-4}$ GeV [15, 16].

A number of searches have been proposed at the LHC to discover $H^{\pm\pm}$ using multi-lepton signatures. The searched modes in [15–17, 31] are pair and associated production with the $H^{\pm\pm}$ decaying into leptonic or gauge boson states. Below we discuss the existing constraints on $H^{\pm\pm}$ from LEP and LHC searches.

- Constraint from LEP-II: The search for doubly-charged Higgs boson $H^{\pm\pm}$ decaying into charged leptons have been performed at LEP-II. This constrains the mass parameter $M_{H^{\pm\pm}} > 97.3$ GeV [35] at 95% C.L.
- Constraints from pair and associated production: Stringent constraint on the $M_{H^{\pm\pm}}$ by analyzing $H^{\pm\pm} \rightarrow l^\pm l^\pm$ have been placed at the 13 TeV LHC. The CMS collaboration looked for different leptonic flavors including $ee, e\mu, e\tau, \mu\mu, \mu\tau$ and $\tau\tau$. In addition, the CMS searches also include the associated production $pp \rightarrow H^{\pm\pm} H^\mp$ and the subsequent decays, $H^\pm \rightarrow l^\pm \nu$. This combined channel of pair-production and associated production gives the stringent constraint $M_{H^{\pm\pm}} > 820$ GeV [25] at 95% C.L for e, μ flavor. The constraint from ATLAS searches comes from pair-production. The bound is $M_{H^{\pm\pm}} > 870$ GeV at 95% C.L [24]. Note that these limits are valid only for a small triplet vev $v_\Delta < 10^{-4}$ GeV.

- Constraint from VBF: For larger values of the triplet vev $v_\Delta \geq 10^{-4}$ GeV, the leptonic branching ratio becomes smaller. Instead the decay mode $H^{\pm\pm} \rightarrow W^\pm W^\pm$ is dominant. Therefore the searches in vector boson fusion (VBF) become more important. A search for $pp \rightarrow jjH^{\pm\pm} \rightarrow jjW^\pm W^\pm$ at the 8 TeV LHC in the VBF channel sets a constraint on the triplet vev $v_\Delta \sim 25$ GeV for $M_{H^{\pm\pm}} \sim 300$ GeV [26]. This constraint has been updated [27] using 13 TeV data at the LHC.

Note that, for extremely small v_Δ , the mass of the doubly-charged Higgs boson is very tightly constrained from pair-production searches. For a larger triplet vev, this constraint significantly relaxes. The VBF cross-section scales quadratically with the triplet vev and hence, increases for a very large vev. However, the range of $v_\Delta \sim 10^{-4} - 10^{-1}$ GeV cannot be probed at the 13 TeV LHC in VBF channel, as the cross-section becomes extremely small in this range. Recently, in [32], the authors have looked for pair-production of $H^{\pm\pm}$ in large v_Δ region and analyzed the signature where the final state contains di-lepton, multi-jet, and missing energy. The lighter mass $M_{H^{\pm\pm}} \lesssim 190$ GeV can be probed at the 14 TeV LHC with 3000 fb^{-1} of data. In [30], the authors have used LHC 8 TeV run-I result of same-sign di-lepton to derive a bound $M_{H^{\pm\pm}} \geq 84$ GeV, relevant for large v_Δ . For large mass of the doubly-charged Higgs, the LHC cross-section however becomes significantly smaller, as shown in Fig. 2. On the other hand, the fall in the cross-section at a e^+e^- collider is relatively smaller. This motivates us to explore the signatures of doubly-charged Higgs at a lepton collider, where the cross-section still remains larger for heavy charged Higgs masses. In the following sections, we explore the scope of a future linear collider to probe large v_Δ region with a) a very low mass range of $H^{\pm\pm}$, that is still experimentally allowed, and b) a very heavy highly boosted $H^{\pm\pm}$.

4 Large triplet vev and collider signatures

In this section, we analyze the collider signatures of a doubly-charged Higgs boson at an e^+e^- collider and explore the sensitivity reach to probe low and high mass regimes. Throughout our analysis, we consider a large triplet vev $v_\Delta \geq 10^{-4}$ GeV, where the present experimental constraints are weak. As the prototype example, we consider CLIC [36–39] that will operate with three different center of mass energies $\sqrt{s} = 380, 1400$ GeV and 3 TeV. We present our simulation for 380 GeV and 3 TeV center of mass energies. The doubly-charged Higgs boson, $H^{\pm\pm}$, can be produced at e^+e^- collider via photon and Z -boson mediated diagrams, as shown in Fig. 1. We show in Fig. 2 the respective production cross-sections. As both of the diagrams are s-channel processes, the cross-section reduces with increasing center of mass energy. For a relatively small center of mass energy $\sqrt{s} = 380$ GeV, the maximum cross-section reaches up to $\sigma \sim 506 \text{ fb}$ for $M_{H^{\pm\pm}} = 102$ GeV. A rapid decline in the cross-section occurs near $M_{H^{\pm\pm}} \sim 190$ GeV, close to kinematical threshold. For the choice of large v_Δ , the produced particles $H^{\pm\pm}$ will decay into $W^\pm W^\pm$ gauge bosons with almost 100% branching ratio. In the following, we will first discuss the low-mass regime, that can be probed in the $\sqrt{s} = 380$ GeV run. Following that we discuss the high-mass regime, that can be explored at 3 TeV center of mass energy and gives rise to specific signatures of boosted Higgs boson. In both cases we focus on multi-jet final states.

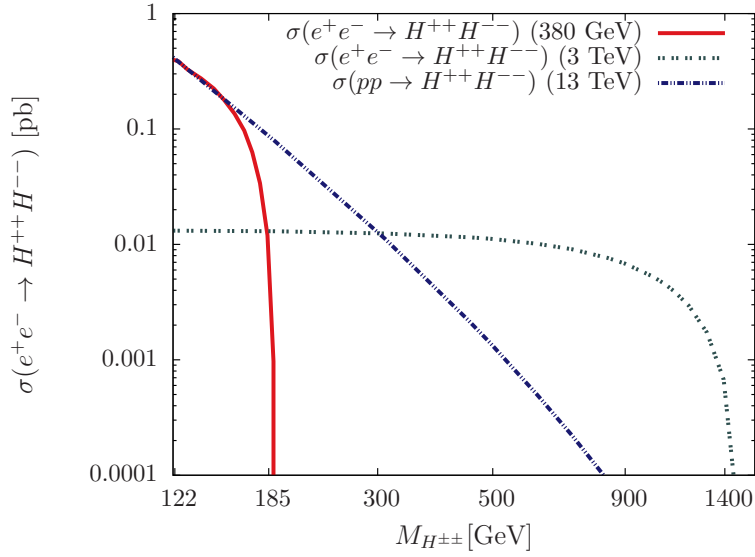


Figure 2. The production cross-section at e^+e^- collider. The center of mass energies are $\sqrt{s} = 380$ GeV and 3 TeV. For comparison, we also show the cross-section at 13 TeV LHC. The pair-production cross-section increases by a factor of two, if CLIC uses 80%, and 30% beam polarization for electron and positron beam.

4.1 Low mass $H^{\pm\pm}$ at $\sqrt{s} = 380$ GeV

We consider the pair-production of $H^{\pm\pm}$, and its subsequent decay into $W^\pm W^\pm$ at $\sqrt{s} = 380$ GeV. The produced W^\pm decay dominantly into hadronic final states. Thus, to retain as much signal rate as possible, we focus on fully hadronic channel. Therefore, our model signature comprises of multi-jet events. In the subsequent analysis, we demand a high jet multiplicity, i.e., the number of jets $N_{\text{jet}} \geq 7$. For the signal, the production processes are

- $e^+e^- \rightarrow H^{\pm\pm}H^{\mp\mp} \rightarrow 4W \geq 7j$ for $M_{H^{\pm\pm}} \gtrsim 2M_W$
- $e^+e^- \rightarrow H^{\pm\pm}H^{\mp\mp} \rightarrow W^\pm jj W^\mp jj \geq 7j$ for $M_{H^{\pm\pm}} < 2M_W$

In the former scenario the $H^{\pm\pm}$ decays predominantly into on-shell $W^\pm W^\pm$, while in the latter case $H^{\pm\pm}$ decays into one on-shell and one off-shell gauge bosons with subsequent decays into jets.

To simulate the events, we use first **FeynRules** [73] and generate the model file via Universal Feynrules Output (UFO) [74, 75]. We compute the hard processes with the package **MadGraph5_aMC@NLO** [76], and pass the output (in LHE format) through **Pythia 6** [77] for showering and hadronization. The detector simulation has been taken into account by **Delphes-3.3.0** [78], where we use the ILD card. Here we use anti- k_t jet clustering algorithm [79] to form jets. Similar final states will be generated from a number of SM processes. We consider the following sets of backgrounds and perform a detailed simulation:

- $e^+e^- \rightarrow t\bar{t} \rightarrow 6j$

$e^+e^- \rightarrow H^{++}H^{--} \rightarrow N_j \geq 7j$			
Mass (GeV)	σ_p (fb)	$\sigma_d(N_j \geq 7j)$ (fb)	$\sigma_d(N_j \geq 7j + b \text{ veto})$ (fb)
121	0.80	0.30	0.20
137	2.08	0.94	0.66
159	5.45	2.58	1.82
172	5.04	2.48	1.74
184	1.11	0.53	0.38
Backgrounds			
Processes	σ_p (fb) $\times 10^{-2}$	$\sigma_d(N_j \geq 7j)$ (fb) $\times 10^{-2}$	$\sigma_d(N_j \geq 7j + b \text{ veto})$ (fb) $\times 10^{-2}$
$e^+e^- \rightarrow t\bar{t} \rightarrow 6j$	10341.0	338.0	36.0
$W^+W^-3j, W^\pm \rightarrow 2j$	8.89	1.18	0.88
$ZZ + 3j, Z \rightarrow 2j$	0.98	0.13	0.10
$7j$	30.32	1.13	0.88
$W^\pm + 5j, W^\pm \rightarrow jj$	30.18	4.64	3.54
$Z + 5j, Z \rightarrow jj$	18.32	2.15	1.61

Table 1. The cross-sections for the signal and background for the fully hadronic final states, arising from $e^+e^- \rightarrow H^{\pm\pm}H^{\mp\mp}$. σ_p refers to the partonic cross-section. σ_d is the cross-section after taking into account detector effects. The last column represents the cross-section with b -veto. The center of mass energy is $\sqrt{s} = 380$ GeV and kinematic cuts are specified in the text.

- $e^+e^- \rightarrow W^+W^- + 3j, W^\pm \rightarrow 2j$, and $e^+e^- \rightarrow ZZ + 3j, Z \rightarrow 2j$
- $e^+e^- \rightarrow 7j$
- $e^+e^- \rightarrow W^\pm + 5j, W^\pm \rightarrow jj$, and $e^+e^- \rightarrow Z + 5j, Z \rightarrow jj$

Among the backgrounds, $e^+e^- \rightarrow 7j$ includes diagrams of coupling order $\alpha_{EW}^2\alpha_S^5$ with quarks and gluons as intermediate particles. As listed above, we treat the $t\bar{t}$ and gauge boson mediated backgrounds separately. For the partonic event generation, we implement the following sets of cuts at MadGraph level both for the signal and backgrounds: the transverse momentum of light jets $p_T(j_i) > 20$ GeV for all the final state partons, the pseudo-rapidity $|\eta| < 5.0$, and the separation between the light jets $\Delta R(j_i, j_j) > 0.4$.

We consider few illustrative mass points between $M_{H^{\pm\pm}} \sim 121$ GeV and the kinematic threshold $M_{H^{\pm\pm}} \sim 184$ GeV, and display the signal cross-sections in Table. 1. The cross-sections σ_p refers to the partonic cross-section, while σ_d is after taking into account reconstruction and detector effects. In addition to the cuts at the partonic level, we further implement few more selection cuts: the transverse momentum of jets $p_T(j_i) > 20$ GeV for all the jets, pseudo-rapidity $|\eta| < 4.5$ for jets, and the number of jets $N_j \geq 7j$. The largest background arises from $t\bar{t} \rightarrow 6j$, where the cross-section is about 103 fb at the partonic level. This is much larger than the largest signal cross-section 5.45 fb, corresponding to $M_{H^{\pm\pm}} = 159$ GeV. For other mass points, the ratio is even bigger. However, demanding high jet multiplicity $N_j \geq 7j$ reduces this background to $\sigma_d \sim 3$ fb. For the masses of the

doubly-charged Higgs boson $M_{H^{\pm\pm}} = 159$ and 172 GeV, the signal and background cross-sections become almost equal after demanding higher jet multiplicity. A few comments are in order:

$e^+e^- \rightarrow H^{++}H^{--} \rightarrow N_j \geq 7j$		
Mass (GeV)	n_s	\mathcal{L} (fb $^{-1}$)
121	1.54	1054.14
137	4.48	124.56
159	10.48	22.76
172	10.15	24.26
184	2.65	355.99

Table 2. The statistical significance n_s for $\mathcal{L} = 100$ fb $^{-1}$. The third column displays the required luminosity to achieve 5σ significance. The center of mass energy is $\sqrt{s} = 380$ GeV.

- Between the higher and lower mass ranges, i.e., $M_{H^{\pm\pm}} > 2M_W$ and $M_{H^{\pm\pm}} < 2M_W$, the former scenario corresponds to larger pair-production cross-sections. The fall in cross-section in the higher mass range occurs when $M_{H^{\pm\pm}} \sim 184$ GeV, where it approaches the kinematic threshold. For lower mass ranges, $M_{H^{\pm\pm}} \sim 121$ GeV, the reduction of cross-section after the detector effect occurs due to stronger kinematic cuts. The produced jets from a $H^{\pm\pm}$ with mass $M_{H^{\pm\pm}} \sim 121$ GeV are often quite soft. With the constraint on jet transverse momentum $p_T > 20$ GeV the reconstruction efficiency becomes smaller.
- The signal comprises of hadronic final states with higher jet multiplicity. For the signal, $H^{\pm\pm}$ decays into two W^\pm with subsequent decay into quarks, resulting in a final state with $N_j = 8$. At a e^+e^- collider, there are only a few SM processes that can generate a similar final state. A full reconstruction of the signal results in a fairly low reconstruction efficiency. Thus, we allow for one jet to be too soft or out of the kinematic cuts range.

In Table. 2, we derive the statistical significance $n_s = \sigma_d(S)\sqrt{\mathcal{L}}/\sqrt{\sigma_d(S) + \sigma_d(B)}$ for our benchmark points corresponding to Table. 1. Here $\sigma_d(S)$ and $\sigma_d(B)$ represent the final

$e^+e^- \rightarrow H^{++}H^{--} \rightarrow N_j \geq 7j + b \text{ veto}$		
Mass (GeV)	$n_s(b)$	\mathcal{L} (fb $^{-1}$)
121	2.52	393.67
137	6.33	62.39
159	12.14	16.96
172	11.84	17.83
184	4.23	139.72

Table 3. The statistical significance $n_s(b)$ for $\mathcal{L} = 100$ fb $^{-1}$ and the required luminosity to achieve 5σ significance, after implementing the b -veto. The center of mass energy is $\sqrt{s} = 380$ GeV.

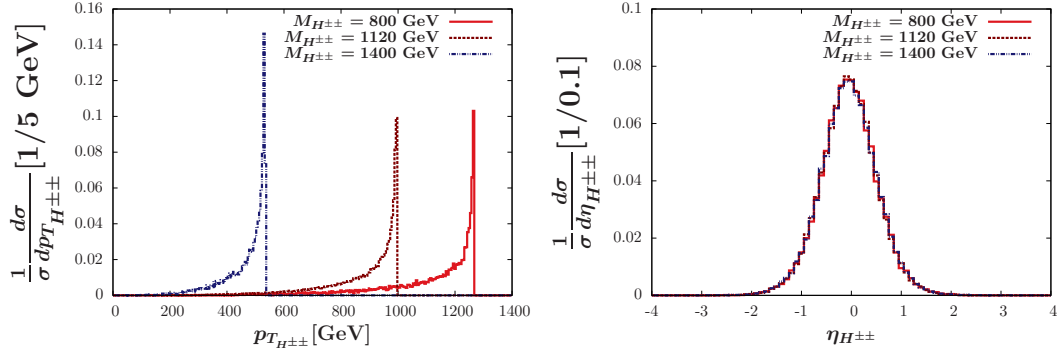


Figure 3. The normalized distribution of the transverse momentum and the pseudo-rapidity for the produced $H^{\pm\pm}$.

cross-sections for the signal and background after all the selection cuts. Additionally, we also show the required luminosity to achieve a 5σ significance. Other than the extreme low and high mass ranges $M_{H^{\pm\pm}} = 121$ and 184 GeV, all other mass points have a large discovery prospect with 124 fb^{-1} of data. In particular, we show that the doubly-charged Higgs boson with intermediate masses of 159 GeV (172 GeV) can be discovered with 5σ significance with only $\mathcal{L} \sim 22$ (24) fb^{-1} , respectively. This further improves to $\mathcal{L} \sim 16$ (17) fb^{-1} after applying a b -veto ($50 - 60\%$ efficiency and 1% miss-tag efficiency), that helps in reducing the dominant top-quark pair background.

4.2 Boosted Heavy $H^{\pm\pm}$ at $\sqrt{s} = 3$ TeV

We now consider heavy $H^{\pm\pm}$ with a mass $M_{H^{\pm\pm}} \sim 1$ TeV and its decay into like-sign $W^\pm W^\pm$ gauge bosons. The produced W^\pm decays into hadronic as well as leptonic states. As before, we focus on the purely hadronic final states, which has the largest branching ratio. For such heavy $H^{\pm\pm}$, each of the produced W^\pm boson will have large transverse momentum. For a 1.1 TeV $H^{\pm\pm}$, their transverse momentum peaks around $p_T \sim 1$ TeV, and most of the W^\pm are produced in the central region. We show the transverse momentum, and the pseudo-rapidity distribution of $H^{\pm\pm}$ in Fig. 3, for the illustrative benchmark points $M_{H^{\pm\pm}} = 800$ GeV, 1120 GeV and 1.4 TeV.

The final decay products of such heavy Higgs bosons are highly collimated, and can be reconstructed as fat-jets, see Fig. 4. Therefore, our model signature for such high mass $H^{\pm\pm}$ is

- $e^+e^- \rightarrow H^{\pm\pm}H^{\mp\mp} \rightarrow W^\pm W^\mp W^\pm W^\mp \rightarrow 4 \text{ fat-jet}$.

To generate signal and backgrounds we use the same tool-chain as in Sec. 4.1 except the use of Delphes. Here we analyze the output of **Pythia 8** [80] (in **HepMC** [81] format) and recluster fat-jets using Cambridge-Aachen algorithm [82] in **FastJet-3.0.0** [83] with radius parameter $R = 1.0$. In Fig. 5, we show the transverse momentum of the leading fat-jet j_1 and the 4th leading fat-jet j_4 . A number of backgrounds can lead to the final states

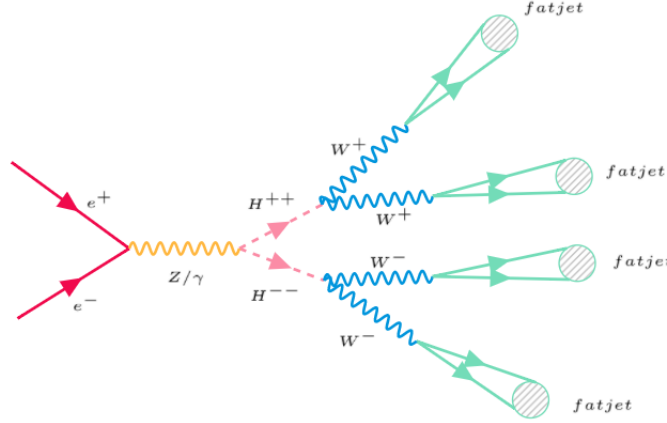


Figure 4. The Feynman diagram for $H^{++}H^{--}$ pair-production and its subsequent decays to 4 fat-jet.

with multiple fat-jets. These are: $4j$ (includes both the QED and QCD contributions), W^+W^-2j , and W^+/W^-3j , W^+W^-Zjj and $t\bar{t}$, with subsequent decays of W boson and the top quark into jets. The partonic cross-sections of the signal and backgrounds are shown in Table. 4. The cross-sections for W^+W^-Zjj and $t\bar{t}$ are small compared to other backgrounds. Therefore, we do not include these backgrounds in our final analysis. Below we discuss in detail the pre-selection and selection cuts for the signal and backgrounds:

- Most of the signal events are in the central region with pseudo-rapidity distributed around $\eta_{H^{\pm\pm}} \sim 0$, as can be seen in Fig. 3. Additionally, the signal jets have a very high H_T (scalar sum of transverse momentum of all final state particles), as shown in Fig. 6. We consider no cuts on the signal at the parton level. While generating the backgrounds, we consider the following partonic cuts for $4j$ - the transverse momentum of the jets $p_T > 60$ GeV, and the jet-jet separation $\Delta R(j, j) > 0.6$;

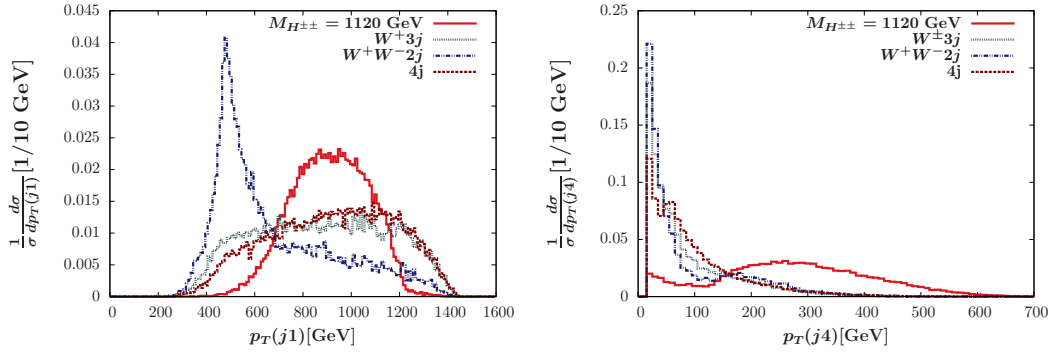


Figure 5. The p_T distribution of the leading and 4th leading fat-jets. For signal, we consider $M_{H^{\pm\pm}} = 1120$ GeV.

$e^+e^- \rightarrow H^{++}H^{--} \rightarrow W^+W^+W^-W^- \rightarrow Nj_{\text{fat}}$							
Masses (GeV)	σ_p (ab)	$4j_{\text{fat}} (> 120 \text{ GeV})$	4 MD	1 tagged	2 tagged	3-tagged	4-tagged
800	1250	812.9	758.0	757.9	748.9	671.8	389.0
1000	850.6	527.0	492.5	492.3	486.1	436.6	258.9
1120	670.0	380.0	358.4	358.3	354.2	321.9	193.1
1350	167.1	80.4	75.54	75.52	74.88	68.2	42.0
1400	94.36	45.54	42.85	42.84	42.42	38.6	24.0

Backgrounds							
Processes	σ_p (ab)	$4j (> 120 \text{ GeV})$	4 MD	1 tagged	2 tagged	3-tagged	4-tagged
$4j$	6900.0	1310.0	895.0	360.0	68.0	5.5	0.0
$W^+3j \text{ \& } W^-3j$	1900.0	320.0	220.0	166.0	44.0	4.8	1.52×10^{-1}
W^+W^-2j	190.0	25.6	17.7	15.6	8.3	1.23	5.7×10^{-2}
W^+W^-Zjj	4.23	-	-	-	-	-	-
$t\bar{t}$	42	-	-	-	-	-	-

Table 4. The cut-flow for the signal and backgrounds. The cross-sections are in fb. σ_p refers to the partonic cross-section. In the backgrounds the decays of the W^\pm boson and top quark to jets are included. Here MD refers to Mass-drop. See text for details.

for $W^+W^-2j(W^\pm > 2j)$ and $W^+3j(W^\pm > 2j)$ - $p_T > 60$ GeV for the leading 4-jets, the transverse momentum $p_T > 20$ GeV for the remaining jets, and the jet-jet separation $\Delta R(j, j) > 0.4$. The H_T and pseudo-rapidity cut is the same for all the backgrounds, $H_T > 1000$ GeV and $|\eta| < 2.5$. For $t\bar{t}$ samples we have put $\Delta R(b, j) > 0.4$ separation cut and transverse momentum cut on leading two light jet as $p_T > 60.0$ GeV. Additionally, we also demand p_T of the bottom quarks more than 60 GeV and the p_T of the remaining light quarks more than 20 GeV.

- The ΔR separation of the produced W^+W^+ , W^+W^- are shown in Fig. 7. It is evident that for relatively lower masses of $H^{\pm\pm}$, such as 800 GeV, the W^+ and W^+ are closer, as compared to 1400 GeV. This occurs as the $H^{\pm\pm}$ with 800 GeV mass

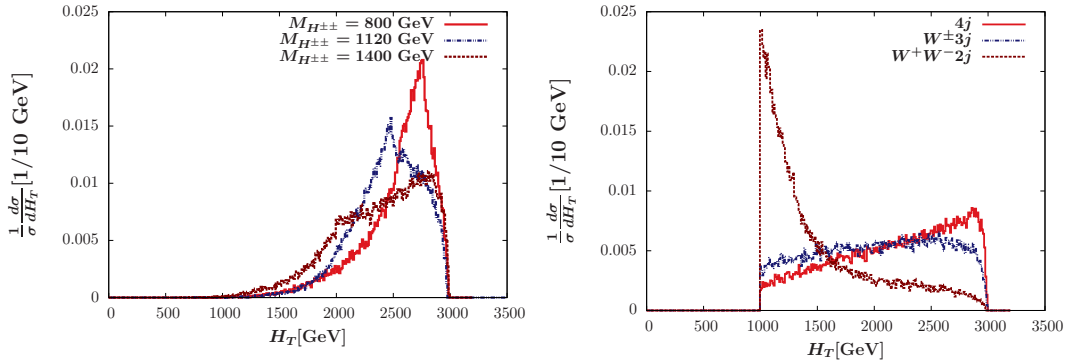


Figure 6. The H_T distribution of the jets at the partonic level. We consider three illustrative benchmark points $M_{H^{\pm\pm}} = 800, 1120, \text{ and } 1400$ GeV.

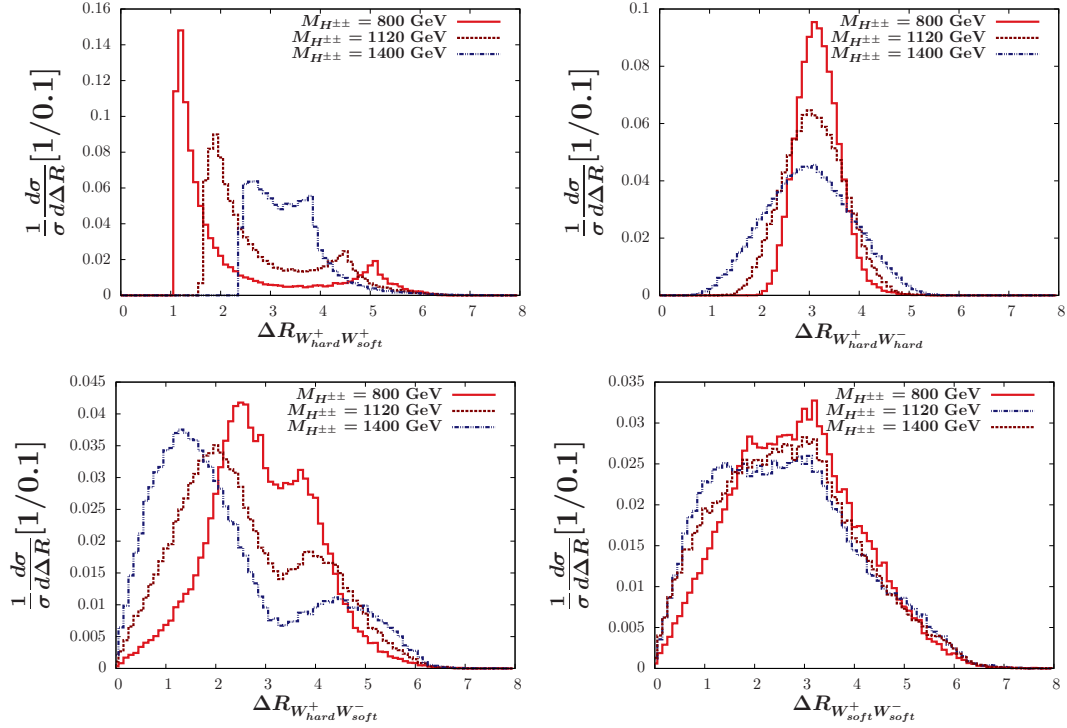


Figure 7. The ΔR_{WW} distribution of the different W^\pm , produced from the doubly charge Higgs $H^{\pm\pm}$. The W 's in this figure are p_T ordered.

is more boosted than the higher mass $H^{\pm\pm}$. Hence, the produced $W^{\pm\pm}$ are more collimated.

- The model signature contains four fat-jet with high momentum. We show in Fig. 5, the transverse momentum of leading and 4th leading fat-jet for $M_{H^{\pm\pm}} = 1120$ GeV. Additionally, we also show the distributions of the backgrounds. It is evident that most of the jets have larger transverse momentum for signal, with $p_T \gg 100$ GeV. Therefore, we design our selection cuts as a) the number of fat-jets $N_{j_{\text{fat}}} = 4$, b) $p_{T_{j_{\text{fat}}}} > 120$ GeV for all the fat-jets.
- We further carry out substructure analysis for the fat-jets. To reconstruct the W bosons we use the mass-drop tagger [84] of which compares the energy-sharings of subjets to indicate if the fat-jet was initiated by a W boson or a parton. For the signal and background, we show the invariant mass of the two sub-jets inside the fat-jet in Fig. 8. For the signal, the subjets inside a fatjet are generated from the W . Therefore, the distribution peaks around the W mass. For the different backgrounds, $4j$ gives flat distribution, while W^+W^-2j and W^+3j shows smaller peak around M_W . As shown in Table. 4, the backgrounds are significantly reduced after applying the selection cut $|M_{j_1j_2} - M_W| \leq 20$ GeV. Here, $M_{j_1j_2}$ is the invariant mass of the subjets j_1 and j_2 inside a fat-jet. A detailed cut-flow chart is given in Table. 4. If at

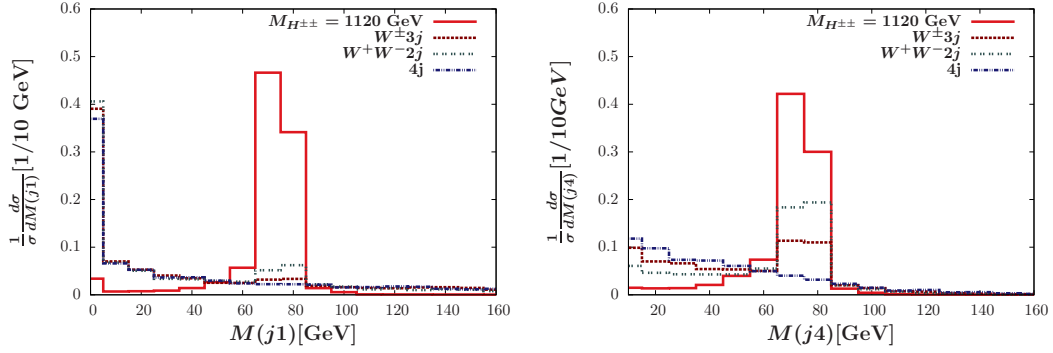


Figure 8. The invariant mass of the fat-jet(leading and 4th leading) constructed using sub-jets four momentum. For signal, we consider $M_{H^{\pm\pm}} = 1120$ GeV.

least one fat-jet passes the invariant mass selection cut, we have 1-tagged event; if at least two fat-jet pass the cut, we have 2-tagged event and so on.

From Table. 4, the effect of the substructure analysis is clearly evident. The largest background arises from the $e^+e^- \rightarrow 4j$ events. At the partonic level we find a cross-section of $\sigma_p(4j) \sim 6.9 \text{ fb} \gg \sigma_p(\text{signal})$. The higher transverse momentum cut on jet p_T reduces the signal nominally, and the background by more than $\mathcal{O}(5)$ for $4j, WW2j$ and $W + 3j$. Demanding that 4 fat-jets have a non-trivial substructure (referred to as mass-drop MD in Table. 4) reduces the background even more. Finally, with the invariant mass cut for the subjets, all backgrounds become almost negligible. For the $H^{\pm\pm}$ masses between 800 GeV to 1.1 TeV one can achieve a $S/B \sim \mathcal{O}(10)$. We show the required luminosity to achieve a discovery in Table. 5. The 800-1120 GeV doubly-charged Higgs boson can be discovered with 39 - 95 fb^{-1} of data with at least 2 fat-jet tagged as W-bosons. However, for higher masses, such as 1.4 TeV a minimum 3 tagged jets will be required.

$e^+e^- \rightarrow H^{++}H^{--} \rightarrow W^+W^+W^-W^- \rightarrow Nj_{\text{fat}}$		
Masses (GeV)	n_s (2, 3-tagged $\mathcal{L} = 500 \text{ fb}^{-1}$)	$\mathcal{L}(\text{fb}^{-1})$ (with 2,3-tagged)
800	17.96(2-tag)	38.75
1000	13.95(2-tag)	64.23
1120	11.49(2-tag)	94.68
1350	5.40(3-tag)	428.66
1400	3.85(3-tag)	843.31

Table 5. The statistical significance n_s for $\mathcal{L} = 500 \text{ fb}^{-1}$ and the required luminosity to achieve 5σ significance. The c.m.energy is $\sqrt{s} = 3 \text{ TeV}$. In the 2nd column, to derive significance, we consider 2 tagged events for 800-1120 GeV mass range and 3 tagged events for the higher mass range. Here 2-tag implies two or more than two fat-jet masses are within the window of 60-100 GeV, and the fat-jets are tagged as W jets. Similar criteria applies for 3-tagged jets.

5 Discussion and Conclusions

The Type-II seesaw model consists of an extension of the scalar sector by a Higgs triplet field Δ with hypercharge $Y = +2$. The neutral component of the triplet acquires a vev and generates the light neutrino mass. One of the most attractive features of this model is the presence of the doubly-charged Higgs boson $H^{\pm\pm}$. Depending on the triplet vev, $H^{\pm\pm}$ can decay into a number of final states, including same-sign leptons, same sign gauge bosons, and via cascade decay to three body final states. For the lower triplet vev where $H^{\pm\pm} \rightarrow l^\pm l^\pm$ decays are predominant, the doubly-charged Higgs boson mass is tightly constrained by LHC pair and associated production searches, $M_{H^{\pm\pm}} > 820, 870$ GeV. However, the higher triplet vev region is poorly constrained by the VBF searches. Moreover, the LHC search is limited in the very high mass region $M_{H^{\pm\pm}} \sim 1$ TeV, where the cross-section is tiny.

In this work, we consider an e^+e^- collider operating with two center of mass energies $\sqrt{s} = 380$ GeV and 3 TeV, and probe the large v_Δ region $v_\Delta \geq 10^{-2}$ GeV. We consider two mass regimes, a) light $H^{\pm\pm}$ with mass $M_{H^{\pm\pm}} \lesssim 180$ GeV, and b) a very heavy $H^{\pm\pm}$ with mass $M_{H^{\pm\pm}} \sim 800 - 1400$ GeV. We consider fully hadronic decays of the produced W 's and perform a detailed analysis for the multi-jet final states.

For the 380 GeV center of mass energy, we look into multi-jet final states with $N_j \geq 7j$. We find that a doubly-charged Higgs boson with mass $M_{H^{\pm\pm}} \sim 160 - 172$ GeV can be discovered in the immediate run of the e^+e^- collider, with only integrated luminosity $\mathcal{L} \sim 24 \text{ fb}^{-1}$. This improves considerably once we apply a b -veto, reducing the $t\bar{t}$ background to $\sigma \sim \mathcal{O}(0.1)$ fb.

The higher mass range $M_{H^{\pm\pm}} \geq 1$ TeV can be probed in the $\sqrt{s} = 3$ TeV run of the e^+e^- collider. Note that, for such high masses of $H^{\pm\pm}$ the pair-production cross-section at 13 TeV LHC is significantly smaller. Therefore, an e^+e^- collider with large center of mass energy is more suitable to probe the high mass range. For such heavy mass, the produced W s are boosted and their subsequent decay products will be collimated, resulting in fat-jets. A number of SM processes, including $4j$, $W^\pm 3j$, $W^\pm W^\pm 2j$ can mimic the signal. To reduce backgrounds, we carry out a jet-substructure analysis with W -tagging. We find that for the 800-1120 GeV mass range, a minimum of two tagged jets can effectively reduce the total backgrounds to a level of $\sigma \sim \mathcal{O}(0.1)$ fb, whereas the signal cross-section is $\sigma \sim \mathcal{O}(0.3 - 0.7)$ fb. For higher masses, three tagged jets are needed. A doubly-charged Higgs boson with mass between 800-1120 GeV can be discovered with $\mathcal{L} \lesssim 95 \text{ fb}^{-1}$ of data. For even higher masses, such as $M_{H^{\pm\pm}} \sim 1400$ GeV, a discovery will require much higher integrated luminosities.

Thus, a future high-energy e^+e^- collider can provide an outstanding opportunity to probe weakly-coupled heavy particles, which are beyond the reach of the LHC.

Acknowledgments

MM acknowledges the support of the DST-INSPIRE research grant IFA14-PH-99, and the cluster facility of Institute of Physics (IOP), Bhubaneswar, India. MM thanks the

workshop ‘Physics at CLIC’, held during July 17th-18th at CERN, Geneva, where part of the work has been carried out. SS acknowledges the funding assistance provided by Royal Society International Exchange program and the hospitality of the Institute for Particle Physics Phenomenology (IPPP) at Durham University where part of the work has been carried out.

References

- [1] S. Weinberg, *Baryon and Lepton Nonconserving Processes*, *Phys. Rev. Lett.* **43** (1979) 1566–1570.
- [2] F. Wilczek and A. Zee, *Operator Analysis of Nucleon Decay*, *Phys. Rev. Lett.* **43** (1979) 1571–1573.
- [3] P. Minkowski, $\mu \rightarrow e\gamma$ at a Rate of One Out of 10^9 Muon Decays?, *Phys. Lett.* **B67** (1977) 421–428.
- [4] R. N. Mohapatra and G. Senjanovic, *Neutrino Mass and Spontaneous Parity Violation*, *Phys. Rev. Lett.* **44** (1980) 912.
- [5] T. Yanagida, *Horizontal Symmetry and Masses of Neutrinos*, *Conf. Proc.* **C7902131** (1979) 95–99.
- [6] M. Gell-Mann, P. Ramond and R. Slansky, *Complex Spinors and Unified Theories*, *Conf. Proc.* **C790927** (1979) 315–321, [[1306.4669](#)].
- [7] J. Schechter and J. W. F. Valle, *Neutrino Masses in $SU(2) \times U(1)$ Theories*, *Phys. Rev.* **D22** (1980) 2227.
- [8] K. S. Babu, C. N. Leung and J. T. Pantaleone, *Renormalization of the neutrino mass operator*, *Phys. Lett.* **B319** (1993) 191–198, [[hep-ph/9309223](#)].
- [9] S. Antusch, M. Drees, J. Kersten, M. Lindner and M. Ratz, *Neutrino mass operator renormalization in two Higgs doublet models and the MSSM*, *Phys. Lett.* **B525** (2002) 130–134, [[hep-ph/0110366](#)].
- [10] M. Magg and C. Wetterich, *Neutrino Mass Problem and Gauge Hierarchy*, *Phys. Lett.* **B94** (1980) 61–64.
- [11] T. P. Cheng and L.-F. Li, *Neutrino Masses, Mixings and Oscillations in $SU(2) \times U(1)$ Models of Electroweak Interactions*, *Phys. Rev.* **D22** (1980) 2860.
- [12] G. Lazarides, Q. Shafi and C. Wetterich, *Proton Lifetime and Fermion Masses in an $SO(10)$ Model*, *Nucl. Phys.* **B181** (1981) 287–300.
- [13] R. N. Mohapatra and G. Senjanovic, *Neutrino Masses and Mixings in Gauge Models with Spontaneous Parity Violation*, *Phys. Rev.* **D23** (1981) 165.
- [14] R. Foot, H. Lew, X. G. He and G. C. Joshi, *Seesaw Neutrino Masses Induced by a Triplet of Leptons*, *Z. Phys.* **C44** (1989) 441.
- [15] P. Fileviez Perez, T. Han, G.-y. Huang, T. Li and K. Wang, *Neutrino Masses and the CERN LHC: Testing Type II Seesaw*, *Phys. Rev.* **D78** (2008) 015018, [[0805.3536](#)].
- [16] A. Melfo, M. Nemevsek, F. Nesti, G. Senjanovic and Y. Zhang, *Type II Seesaw at LHC: The Roadmap*, *Phys. Rev.* **D85** (2012) 055018, [[1108.4416](#)].

- [17] F. del Aguila and J. A. Aguilar-Saavedra, *Distinguishing seesaw models at LHC with multi-lepton signals*, *Nucl. Phys.* **B813** (2009) 22–90, [[0808.2468](#)].
- [18] S. Chakrabarti, D. Choudhury, R. M. Godbole and B. Mukhopadhyaya, *Observing doubly charged Higgs bosons in photon-photon collisions*, *Phys. Lett.* **B434** (1998) 347–353, [[hep-ph/9804297](#)].
- [19] M. Aoki, S. Kanemura and K. Yagyu, *Testing the Higgs triplet model with the mass difference at the LHC*, *Phys. Rev.* **D85** (2012) 055007, [[1110.4625](#)].
- [20] E. J. Chun and P. Sharma, *Search for a doubly-charged boson in four lepton final states in type II seesaw*, *Phys. Lett.* **B728** (2014) 256–261, [[1309.6888](#)].
- [21] S. Banerjee, M. Frank and S. K. Rai, *Higgs data confronts Sequential Fourth Generation Fermions in the Higgs Triplet Model*, *Phys. Rev.* **D89** (2014) 075005, [[1312.4249](#)].
- [22] A. Arhrib, R. Benbrik, M. Chabab, G. Moulhaka, M. C. Peyranere, L. Rahili et al., *The Higgs Potential in the Type II Seesaw Model*, *Phys. Rev.* **D84** (2011) 095005, [[1105.1925](#)].
- [23] P. S. Bhupal Dev, D. K. Ghosh, N. Okada and I. Saha, *125 GeV Higgs Boson and the Type-II Seesaw Model*, *JHEP* **03** (2013) 150, [[1301.3453](#)].
- [24] ATLAS collaboration, M. Aaboud et al., *Search for doubly charged Higgs boson production in multi-lepton final states with the ATLAS detector using proton-proton collisions at $\sqrt{s} = 13$ TeV*, [1710.09748](#).
- [25] CMS collaboration, *A search for doubly-charged Higgs boson production in three and four lepton final states at $\sqrt{s} = 13$ TeV*, Tech. Rep. CMS-PAS-HIG-16-036, CERN, Geneva, 2017.
- [26] CMS collaboration, V. Khachatryan et al., *Study of vector boson scattering and search for new physics in events with two same-sign leptons and two jets*, *Phys. Rev. Lett.* **114** (2015) 051801, [[1410.6315](#)].
- [27] CMS collaboration, A. M. Sirunyan et al., *Observation of electroweak production of same-sign W boson pairs in the two jet and two same-sign lepton final state in proton-proton collisions at $\sqrt{s} = 13$ TeV*, [1709.05822](#).
- [28] S. Kanemura, K. Yagyu and H. Yokoya, *First constraint on the mass of doubly-charged Higgs bosons in the same-sign diboson decay scenario at the LHC*, *Phys. Lett.* **B726** (2013) 316–319, [[1305.2383](#)].
- [29] S. Kanemura, M. Kikuchi, K. Yagyu and H. Yokoya, *Bounds on the mass of doubly-charged Higgs bosons in the same-sign diboson decay scenario*, *Phys. Rev.* **D90** (2014) 115018, [[1407.6547](#)].
- [30] S. Kanemura, M. Kikuchi, H. Yokoya and K. Yagyu, *LHC Run-I constraint on the mass of doubly charged Higgs bosons in the same-sign diboson decay scenario*, *PTEP* **2015** (2015) 051B02, [[1412.7603](#)].
- [31] M. Mitra, S. Niyogi and M. Spannowsky, *Type-II Seesaw and Multilepton Signatures at Hadron Colliders*, [1611.09594](#).
- [32] D. K. Ghosh, N. Ghosh, I. Saha and A. Shaw, *Revisiting the high-scale validity of Type-II seesaw model with novel LHC signature*, [1711.06062](#).
- [33] C. Englert, P. Schichtel and M. Spannowsky, *Same-sign W pair production in composite Higgs models*, *Phys. Rev.* **D95** (2017) 055002, [[1610.07354](#)].

- [34] C. Hays, M. Mitra, M. Spannowsky and P. Waite, *Prospects for new physics in $\tau \rightarrow l\mu\mu$ at current and future colliders*, *JHEP* **05** (2017) 014, [[1701.00870](#)].
- [35] DELPHI collaboration, J. Abdallah et al., *Search for doubly charged Higgs bosons at LEP-2*, *Phys. Lett.* **B552** (2003) 127–137, [[hep-ex/0303026](#)].
- [36] CLIC PHYSICS WORKING GROUP collaboration, E. Accomando et al., *Physics at the CLIC multi-TeV linear collider*, in *Proceedings, 11th International Conference on Hadron spectroscopy (Hadron 2005): Rio de Janeiro, Brazil, August 21-26, 2005*, 2004, [hep-ph/0412251](#).
- [37] L. Linssen, A. Miyamoto, M. Stanitzki and H. Weerts, *Physics and Detectors at CLIC: CLIC Conceptual Design Report*, [1202.5940](#).
- [38] CLIC DETECTOR AND PHYSICS STUDY collaboration, H. Abramowicz et al., *Physics at the CLIC e^+e^- Linear Collider – Input to the Snowmass process 2013*, [1307.5288](#).
- [39] N. Alipour Tehrani, J.-J. Blaising, B. Cure, D. Dannheim, F. Duarte Ramos, K. Elsener et al., *CLICdet: The post-CDR CLIC detector model*, *CLICdp-Note-2017-001* (Mar, 2017) .
- [40] J.-F. Shen and Z.-X. Li, *Doubly charged Higgs bosons pair production through WW fusion at high-energy e^+e^- linear colliders*, *EPL* **111** (2015) 31001.
- [41] S. Blunier, G. Cottin, M. A. Daz and B. Koch, *Phenomenology of a Higgs triplet model at future e^+e^- colliders*, *Phys. Rev.* **D95** (2017) 075038, [[1611.07896](#)].
- [42] J. Cao and X.-Y. Tian, *Doubly and singly charged Higgs pair production at high-energy e^+e^- linear colliders*, *Int. J. Mod. Phys.* **A31** (2016) 1650056.
- [43] Y.-C. Guo, C.-X. Yue and Z.-C. Liu, *The signatures of doubly charged leptons in future linear colliders*, *J. Phys.* **G44** (2017) 085004, [[1611.08843](#)].
- [44] R. Contino, C. Grojean, D. Pappadopulo, R. Rattazzi and A. Thamm, *Strong Higgs Interactions at a Linear Collider*, *JHEP* **02** (2014) 006, [[1309.7038](#)].
- [45] S. Heinemeyer and C. Schappacher, *Neutral Higgs boson production at e^+e^- colliders in the complex MSSM: a full one-loop analysis*, *Eur. Phys. J.* **C76** (2016) 220, [[1511.06002](#)].
- [46] A. Thamm, R. Torre and A. Wulzer, *Future tests of Higgs compositeness: direct vs indirect*, *JHEP* **07** (2015) 100, [[1502.01701](#)].
- [47] N. Craig, M. Farina, M. McCullough and M. Perelstein, *Precision Higgsstrahlung as a Probe of New Physics*, *JHEP* **03** (2015) 146, [[1411.0676](#)].
- [48] G. Durieux, C. Grojean, J. Gu and K. Wang, *The leptonic future of the Higgs*, *JHEP* **09** (2017) 014, [[1704.02333](#)].
- [49] J. Ellis, P. Roloff, V. Sanz and T. You, *Dimension-6 Operator Analysis of the CLIC Sensitivity to New Physics*, *JHEP* **05** (2017) 096, [[1701.04804](#)].
- [50] R. M. Godbole, C. Hangst, M. Muhlleitner, S. D. Rindani and P. Sharma, *Model-independent analysis of Higgs spin and CP properties in the process $e^+e^- \rightarrow t\bar{t}\Phi$* , *Eur. Phys. J.* **C71** (2011) 1681, [[1103.5404](#)].
- [51] S. S. Biswal, R. M. Godbole, R. K. Singh and D. Choudhury, *Signatures of anomalous VVH interactions at a linear collider*, *Phys. Rev.* **D73** (2006) 035001, [[hep-ph/0509070](#)].
- [52] D. Dannheim, P. Lebrun, L. Linssen, D. Schulte, F. Simon, S. Stapnes et al., *CLIC e^+e^- Linear Collider Studies*, [1208.1402](#).

- [53] B. Ananthanarayan, S. K. Garg, C. S. Kim, J. Lahiri and P. Poulse, *Top Yukawa coupling measurement with indefinite CP Higgs in $e^+e^- \rightarrow t\bar{t}\Phi$* , *Phys. Rev.* **D90** (2014) 014016, [[1405.6465](#)].
- [54] M. Thomson, *Model-independent measurement of the $e^+e^- \rightarrow HZ$ cross section at a future e^+e^- linear collider using hadronic Z decays*, *Eur. Phys. J.* **C76** (2016) 72, [[1509.02853](#)].
- [55] G. Milutinović-Dumbelović, I. Božović-Jelisavčić, C. Grefe, G. Kačarević, S. Lukić, M. Pandurović et al., *Physics potential for the measurement of $\sigma(H\nu\bar{\nu}) \times BR(H \rightarrow \mu^+\mu^-)$ at the 1.4 TeV CLIC collider*, *Eur. Phys. J.* **C75** (2015) 515, [[1507.04531](#)].
- [56] H. Wang and B. Yang, *Top partner production at e^+e^- collider in the littlest Higgs Model with T-parity*, *Adv. High Energy Phys.* **2017** (2017) 5463128, [[1706.02821](#)].
- [57] H. Abramowicz et al., *Higgs physics at the CLIC electron-positron linear collider*, *Eur. Phys. J.* **C77** (2017) 475, [[1608.07538](#)].
- [58] S. Banerjee, B. Bhattacharjee, M. Mitra and M. Spannowsky, *The Lepton Flavour Violating Higgs Decays at the HL-LHC and the ILC*, *JHEP* **07** (2016) 059, [[1603.05952](#)].
- [59] S. Heinemeyer and C. Schappacher, *Charged Higgs Boson production at e^+e^- colliders in the complex MSSM: a full one-loop analysis*, *Eur. Phys. J.* **C76** (2016) 535, [[1606.06981](#)].
- [60] V. Ari, O. Akir and S. Kaday, *Pair Production of New Heavy Leptons with $U(1)'$ Charge at Linear Colliders*, *Int. J. Mod. Phys.* **A29** (2014) 1450055, [[1309.7444](#)].
- [61] L. Xiao-Zhou, M. Wen-Gan, Z. Ren-You and G. Lei, *$WW\gamma/Z$ production in the Randall-Sundrum model at LHC and CLIC*, *Phys. Rev.* **D87** (2013) 056008, [[1303.2307](#)].
- [62] A. Llamas-Bugarin, A. Gutierrez-Rodriguez and M. A. Hernandez-Ruz, *Probing the electromagnetic dipole moments of the tau-neutrino in the $U(1)_{B-L}$ model at the ILC and CLIC energies*, *Phys. Rev.* **D95** (2017) 116008, [[1706.03635](#)].
- [63] C.-W. Chiang, S. Kanemura and K. Yagyu, *Phenomenology of the Georgi-Machacek model at future electron-positron colliders*, *Phys. Rev.* **D93** (2016) 055002, [[1510.06297](#)].
- [64] S. Banerjee, P. S. B. Dev, A. Ibarra, T. Mandal and M. Mitra, *Prospects of Heavy Neutrino Searches at Future Lepton Colliders*, *Phys. Rev.* **D92** (2015) 075002, [[1503.05491](#)].
- [65] S. Antusch, E. Cazzato and O. Fischer, *Sterile neutrino searches at future e^-e^+ , pp , and e^-p colliders*, *Int. J. Mod. Phys.* **A32** (2017) 1750078, [[1612.02728](#)].
- [66] A. Ahriche, S. Nasri and R. Soualah, *Radiative neutrino mass model at the e^-e^+ linear collider*, *Phys. Rev.* **D89** (2014) 095010, [[1403.5694](#)].
- [67] S. Antusch, E. Cazzato and O. Fischer, *Higgs production from sterile neutrinos at future lepton colliders*, *JHEP* **04** (2016) 189, [[1512.06035](#)].
- [68] S. Antusch, E. Cazzato and O. Fischer, *Displaced vertex searches for sterile neutrinos at future lepton colliders*, *JHEP* **12** (2016) 007, [[1604.02420](#)].
- [69] S. S. Biswal and P. S. B. Dev, *Probing left-right seesaw models using beam polarization at an e^+e^- collider*, *Phys. Rev.* **D95** (2017) 115031, [[1701.08751](#)].
- [70] J. Barry, L. Dorame and W. Rodejohann, *Linear Collider Test of a Neutrinoless Double Beta Decay Mechanism in left-right Symmetric Theories*, *Eur. Phys. J.* **C72** (2012) 2023, [[1203.3365](#)].
- [71] Z. Chacko, Y. Cui and S. Hong, *Exploring a Dark Sector Through the Higgs Portal at a Lepton Collider*, *Phys. Lett.* **B732** (2014) 75–80, [[1311.3306](#)].

- [72] J. R. Andersen, M. Rauch and M. Spannowsky, *Dark Sector spectroscopy at the ILC*, *Eur. Phys. J. C* **74** (2014) 2908, [[1308.4588](#)].
- [73] A. Alloul, N. D. Christensen, C. Degrande, C. Duhr and B. Fuks, *FeynRules 2.0 - A complete toolbox for tree-level phenomenology*, *Comput. Phys. Commun.* **185** (2014) 2250–2300, [[1310.1921](#)].
- [74] C. Degrande, C. Duhr, B. Fuks, D. Grellscheid, O. Mattelaer and T. Reiter, *UFO - The Universal FeynRules Output*, *Comput. Phys. Commun.* **183** (2012) 1201–1214, [[1108.2040](#)].
- [75] P. de Aquino, W. Link, F. Maltoni, O. Mattelaer and T. Stelzer, *ALOHA: Automatic Libraries Of Helicity Amplitudes for Feynman Diagram Computations*, *Comput. Phys. Commun.* **183** (2012) 2254–2263, [[1108.2041](#)].
- [76] J. Alwall, R. Frederix, S. Frixione, V. Hirschi, F. Maltoni, O. Mattelaer et al., *The automated computation of tree-level and next-to-leading order differential cross sections, and their matching to parton shower simulations*, *JHEP* **07** (2014) 079, [[1405.0301](#)].
- [77] T. Sjostrand, L. Lonnblad and S. Mrenna, *PYTHIA 6.2: Physics and manual*, [hep-ph/0108264](#).
- [78] DELPHES 3 collaboration, J. de Favereau, C. Delaere, P. Demin, A. Giammanco, V. Lematre, A. Mertens et al., *DELPHES 3, A modular framework for fast simulation of a generic collider experiment*, *JHEP* **02** (2014) 057, [[1307.6346](#)].
- [79] M. Cacciari, G. P. Salam and G. Soyez, *The Anti- $k(t)$ jet clustering algorithm*, *JHEP* **04** (2008) 063, [[0802.1189](#)].
- [80] T. Sjostrand, S. Mrenna and P. Z. Skands, *A Brief Introduction to PYTHIA 8.1*, *Comput. Phys. Commun.* **178** (2008) 852–867, [[0710.3820](#)].
- [81] M. Dobbs and J. B. Hansen, *The HepMC C++ Monte Carlo event record for High Energy Physics*, *Comput. Phys. Commun.* **134** (2001) 41–46.
- [82] Y. L. Dokshitzer, G. D. Leder, S. Moretti and B. R. Webber, *Better jet clustering algorithms*, *JHEP* **08** (1997) 001, [[hep-ph/9707323](#)].
- [83] M. Cacciari, G. P. Salam and G. Soyez, *FastJet User Manual*, *Eur. Phys. J. C* **72** (2012) 1896, [[1111.6097](#)].
- [84] J. M. Butterworth, A. R. Davison, M. Rubin and G. P. Salam, *Jet substructure as a new Higgs search channel at the LHC*, *Phys. Rev. Lett.* **100** (2008) 242001, [[0802.2470](#)].